ADVANCED OPTICAL MATERIALS
www.advopticalmat.de

Room Temperature Electrically Driven Ultraviolet Plasmonic Lasers

Xun Yang, Pei-Nan Ni, Peng-Tao Jing, Li-Gong Zhang, Ren-Min Ma, Chong-Xin Shan, De-Zhen Shen,* and Patrice Genevet**

Plasmonic lasers, which make use of the strong confinement of surface plasmon polaritons (SPPs), are key components to realize ultracompact coherent light sources at deep subwavelength scale. Currently, large metal and radiation losses of their metallic cavities limit electrically driven plasmonic lasers operation mainly at cryogenic temperature, where sufficient gain can be obtained. It is a crucial challenge to accomplish high performance electrically driven plasmonic lasers operated at room temperature. Benefiting from the large exciton binding energy and large oscillator strength of zinc oxide (ZnO) gain media, an optically pumped ultraviolet (UV) plasmonic laser is demonstrated from a hybrid metal–insulator–semiconductor structure, in which a magnesium oxide (MgO) gap layer plays a critical role in reducing the metallic loss. Further optimizing the thickness of the MgO gap layer and ZnO active layer, room temperature electrically driven UV plasmonic lasers with a threshold of 70.2 A cm^{-2} are realized for the first time under the injection of electrical carriers through the metallic electrode of the hybrid structure. Localizing light in subwavelength dimension, this novel type of UV plasmonic nanolasers may find various applications in photolithography, sensing, integrated microfluidic systems for surface sterilizations and nanoscale treatment processes.

1. Introduction

The quest for compact coherent light sources for integration with electronic circuits has never been stopped, mostly driven by their potential applications in information storage, optical communications, and accurate metrologies.[1] Conventional photonic lasers based on dielectric cavities are still restricted both in optical mode volume and physical size by diffraction.[2] On the other hand, surface plasmon polaritons (SPPs), which are coupled excitations consisting of electric charge density waves and electromagnetic fields at the metal-dielectric interface, have been extensively utilized to confine light below the diffraction limit.[3] Coherent light sources at deep subwavelength scale, also dubbed plasmonic lasers, rely on SPPs to implement optical confinement, feedback, and amplification.[4] The subwavelength confinement effect leads to strong light-matter interaction in plasmonic lasers and enables a number of new applications in biosensing, nanophotonics, and quantum information technology.[5] In spite of the ever growing number of research work on this topic, the development of plasmonic lasers is mainly hampered by high absorption loss accompanied with the metallic films supporting SPP propagation.[3c,6] As a result, plasmonic lasers are usually optically driven with high thresholds or at cryogenic temperatures to obtain sufficient gain, limiting their practical applications.[7] Large metal loss has become a bottleneck problem of restricting the operation of plasmonic laser at room temperature. Metal–insulator–semiconductor (MIS) structures, which are essentially hybrid plasmonic waveguides consisting of gain media separated from metallic film by a dielectric gap layer, have been proposed to effectively reduce the metallic loss.[3c,6] Thanks to the strong optical confinement as well as the relatively low metal loss in such MIS structure, plasmonic lasers with robust high operation temperature or even room temperature have been demonstrated in infrared regions.[5,9] Furthermore, great efforts have been made to drive the plasmonic laser into short wavelength region or even ultraviolet (UV) region, for which reason hybrid UV plasmonic nanolasers employing ZnO and GaN as gain media have been reported.[1a,7a,8] However, all of them were realized only under optical pumping. For more realistic and

Dr. X. Yang, Dr. P.-T. Jing, Prof. L.-G. Zhang, Prof. C.-X. Shan, Prof. D.-Z. Shen
State Key Laboratory of Luminescence and Applications
Changchun Institute of Optics, Fine Mechanics and Physics
Chinese Academy of Sciences
Changchun 130033, China
E-mail: shancx@ciomp.ac.cn; shendz@ciomp.ac.cn
Dr. X. Yang, Prof. C.-X. Shan
School of Physics and Engineering
Zhengzhou University
Zhengzhou 450052, China
Dr. P.-N. Ni, Dr. P. Genevet
CRHEA (Centre de Recherche sur l'Hétéro-Epitaxie et ses Applications)
CNRS – Université Côte d'Azur
rue Bernard Gregory, Sophia Antipolis, Valbonne 06560, France
E-mail: patrice.genevet@crhea.cnrs.fr
Prof. R.-M. Ma
State Key Lab for Mesoscopic Physics
School of Physics
Peking University
Beijing 100871, China
The ORCID identification number(s) for the author(s) of this article can be found under https://doi.org/10.1002/adom.201801681.

DOI: 10.1002/adom.201801681

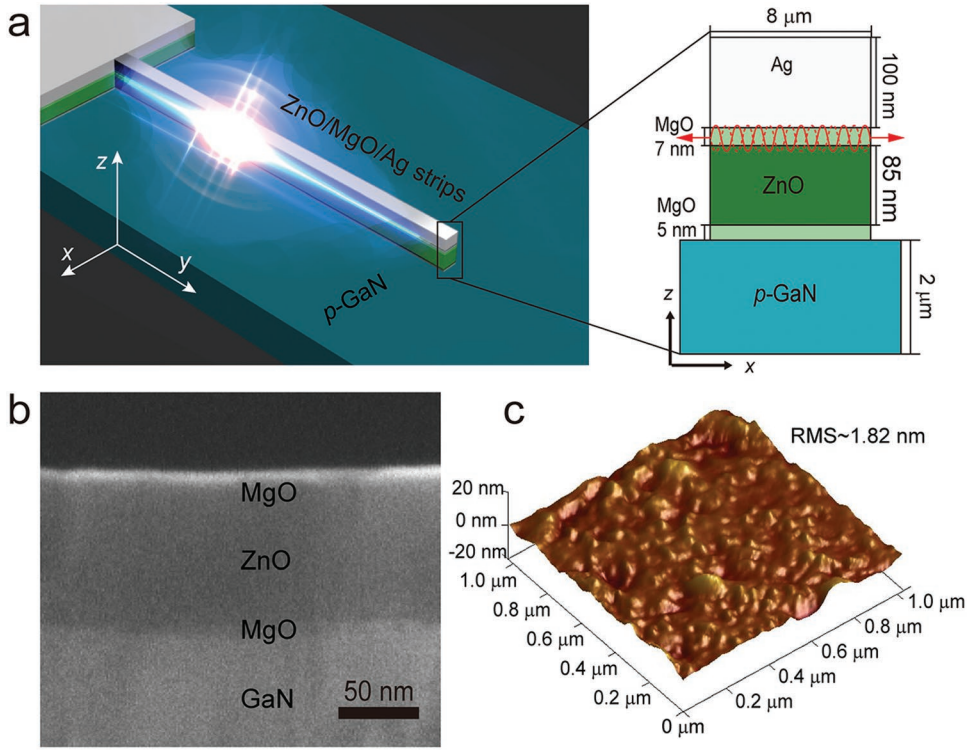

Figure 1. Structure of the electrically driven plasmonic laser. a) The schematic diagram of the p-GaN/MgO/ZnO/MgO/Ag structure. Inset illustrates the SPPs feedback diagram in the ZnO/MgO/Ag cavity. b) Cross-section SEM image of the p-GaN/MgO/ZnO/MgO structure. c) AFM image of an area of 1×1 μm^2 on the as grown GaN/MgO/ZnO/MgO film.

practical applications, room temperature electrically driven UV plasmonic lasers, never reported so far, are eagerly desired.

In this paper, we design and experimentally demonstrate for the first time an electrically driven UV plasmonic laser at room temperature, realized in a p-GaN/MgO/ZnO/MgO/Ag structure (shown in **Figure 1**a). This structure includes a Ag/MgO/ZnO MIS hybrid plasmonic waveguide, in which strong optical confinement and relatively low metal loss can be satisfied simultaneously. Similar strong light confinement mechanism has been reported by Zhang and co-workers[3c] ZnO material is chosen as the gain media due to its significant advantages in fabricating low threshold ultraviolet lasers at room temperature. Its large exciton binding energy and large oscillator strength are also beneficial for coupling with SPPs, corresponding to a faster radiative lifetime.[1a,8,9] The shorter exciton lifetime leads to larger dipole moment, which increase the exciton-SPP energy transfer rate according to a dipole–dipole interaction model.[10] In the proposed epitaxially grown structure, holes are injected into ZnO layer from p-GaN, and electrons are injected from Ag film through MgO gap layer. An additional electron blocking MgO layer has been introduced at the interface between the gain region and the GaN layer to enhance the emission from ZnO by blocking electrons in the ZnO from entering into the p-GaN.[11] An extremely low threshold of 70.2 A cm^{-2} has been achieved in this structure at room temperature, and the output power is reaching 30 μW at an injection current of 40 mA. These figures, amongst the best values ever reported for ZnO based lasers, represent the state-of-the-art performances in electrically driven plasmonic lasers.

2. Results and Discussion

The schematic structure of the plasmonic laser devices is shown in Figure 1a. SPPs propagating along the interface of metal and dielectric form Fabry–Perot (F–P) resonance between the two reflective end-facets of the ZnO/MgO/Ag structure, as shown in the inset of Figure 1a. The state of the art epitaxy technique guarantees uniform thicknesses of each layer, as shown in the scanning electron microscope (SEM) cross-section image of the p-GaN/MgO/ZnO/MgO (Figure 1b). The thickness of the MgO between the ZnO and the GaN, the ZnO gain media and the MgO gap layer is about 5, 85, and 7 nm, respectively. The as-grown film has a very smooth surface with a root-mean-square (RMS) roughness of 1.82 nm measured via atomic force microscopy (AFM) in a 1×1 μm area. Since the Ag film is directly deposited onto the dielectric layer, the smooth surface of the dielectric layer will favor the formation of smooth metallic film at the metal/dielectric interface, reducing considerably the scattering loss of SPPs.[7a,12]

In the epitaxially grown p-GaN/MgO/ZnO/MgO/Ag structure, ZnO layer acts as the gain media. Holes are injected into the ZnO layer from p-GaN, and electrons in Ag film can be injected into the ZnO through the MgO gap layer via direct tunneling effect enhanced through residual material defects (**Figure 2**a). On the other hand, the band alignment characteristic of this structure the MgO layer between GaN and ZnO could block the electrons from entering the GaN side, increasing the optical gain of ZnO layer.[11] Meanwhile, the 7 nm MgO gap layer is introduced to separate Ag from ZnO,

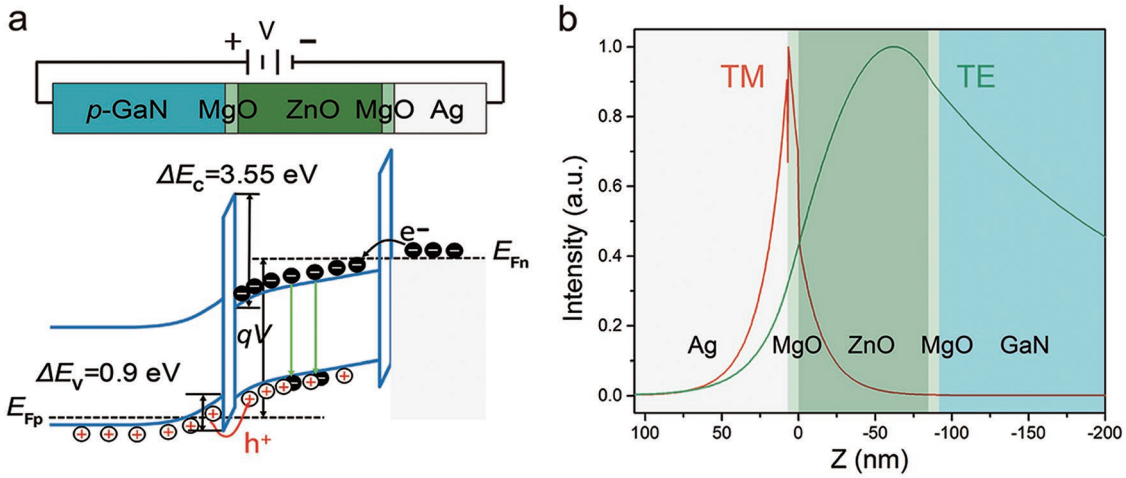

Figure 2. a) Schematic energy band diagram illustrates the emission mechanism of the p-GaN/MgO/ZnO/MgO/Ag structure. b) The simulated electric field distribution for both TM (transverse magnetic, electric field component perpendicular to the Ag film) and TE (transverse electric, electric field component parallel to the Ag film) polarization in the p-GaN/MgO/ZnO/MgO/Ag structure at 396 nm.

forming the Ag/MgO/ZnO MIS hybrid plasmonic structure. The distribution of the electric field in the p-GaN/MgO/ZnO/MgO/Ag structure has been simulated using finite-difference time-domain (FDTD) method, as shown in Figure 2b. The TM mode (transverse magnetic, electric field component perpendicular to the Ag film) is strongly confined at the metal/dielectric interface, while the TE mode (transverse electric, electric field component parallel to the Ag film) is delocalized from the metal surface. Although both TM and TE modes can propagate in the plane, the delocalized TE mode will be scattered out of the plane more efficiently with respect to TM mode since only TM mode can have sufficiently large momentum to hybridize with SPPs.[1d] The exciton transient absorption (TA) spectroscopy is carried out under different pump fluence to investigate the coupling dynamics between SPPs and excitons in the ZnO gain material, as shown in **Figure 3** and Figure S3 in the Supporting Information. Under a low excitation (0.05 mJ cm^{-2}), reduced exciton lifetimes as a result of the excitons-SPPs coupling can be observed from the ZnO/MgO/Ag structure compared with the bare ZnO film. The decays of exciton states can be well fitted by a biexponential decay function corresponding to two relaxation processes, from which the decay time constants of ZnO are fitted to be 52.2 and 701.2 ps, while these two decay time constants of the ZnO/MgO/Ag are 23.6 and 356.9 ps, respectively. The fast relaxation process has been attributed to free exciton decay, and the slow relaxation process is attributed to bound exciton decay. When the pump fluence was increased to the order or more than 0.4 mJ cm^{-2}, the relaxation process becomes ultrafast for the ZnO film, as shown in Figure 3b. This extremely fast process results from the ionization of excitons into electron–hole plasma when the photoexcited exciton density is above the Mott density. However, there is no such observable fast transient from the ZnO/MgO/Ag structure at the similar excitation conditions (Figure 3c), which indicates the stable formation of exciton due to the coupling between excitons and SPPs. Photoluminescence (PL) measurements have also been performed to better understand the carrier relaxation processes inside the hybrid plasmonic structure (Figure S4, Supporting Information). In general, ZnO operates in the electron–hole plasma (EHP) region above 389 nm.[8,13] Nevertheless, in the plasmonic structures (ZnO/Ag and ZnO/MgO/Ag), lasing occurs near the exciton transition energies between 382 and 385 nm.[8] The blueshifts of PL emission wavelength in the plasmonic structures further confirms that the optical gain of

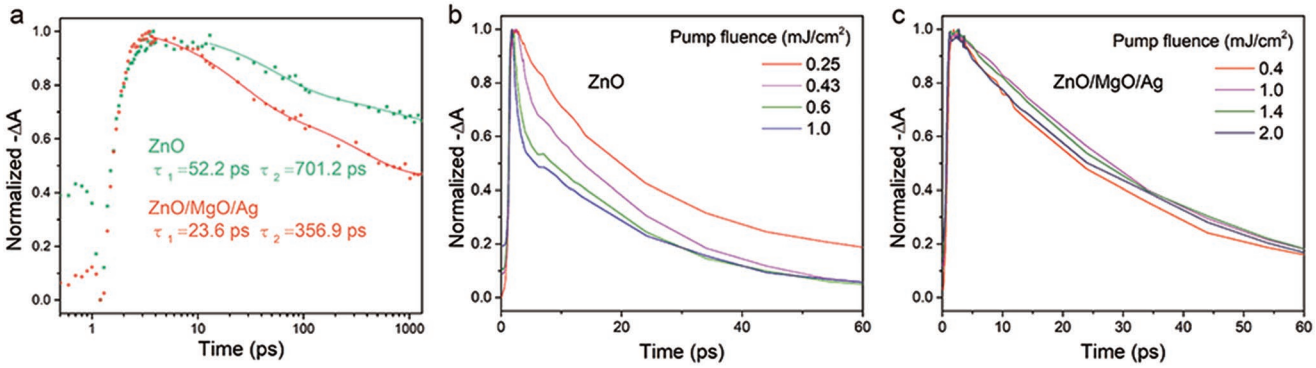

Figure 3. a) TA kinetic traces of the ZnO and ZnO/MgO/Ag structure at pump fluence of 0.05 mJ cm^{-2} probed at 377 nm, corresponding to the exciton absorption. b,c) The TA changes of the ZnO (b) and ZnO/MgO/Ag structure (c) as a function of time under different the pump fluence.

this structure is related to the exciton recombination process. There have been several reports and vivid debates in the literature concerning the gain mechanisms, i.e., excitonic or EHP, responsible for lasing operation of ZnO microlasers. In Figure S4c in the Supporting Information, it is shown that bare ZnO film laser features typical redshift emission, as observed in several reports, probably corresponding to EHP gain. From our experimental evidences, it seems that plasmonic lasers can instead operate in the excitonic regime under the same optical pumping condition. This can be deduced from the dependence of the emission wavelength with respect to the optical pumping fluence. For both Ag/ZnO and ZnO/MgO/Ag plasmonic lasers, the emission is not redshifted. This drastic difference is related to the exciton–plasmons coupling that reduces the radiative lifetime of the excitonic state, damping the carrier density before reaching Mott transition to the EHP regime and forcing the system to operate in the exciton emission regime at relatively high carrier injection density, which agrees very well with the observations from the TA measurements. Meanwhile, the thresholds of the ZnO, ZnO/Ag, and ZnO/MgO/Ag structures being 0.24, 0.81, and 0.51 mJ cm^{-2}, respectively, show that although the plasmonic structure is capable of confining light at subwavelength dimension, the existence of metallic part dramatically increases the lasing thresholds. On the other hand, the spontaneous emission factor, β, which is the proportion of emission coupled into the lasing mode, is also crucial for the lasing behavior since laser threshold is inversely proportional to β factor.[1c] The β factor of the bare ZnO can be derived to be ≈0.01 from the transition kink between spontaneous emission and lasing region in the corresponding light–light (L–L) curve.[3c] In contrast, the measured β factors of the ZnO/Ag and ZnO/MgO/Ag structures are 0.2 and 0.1, respectively, remarkably larger than that of the bare ZnO. Although the ZnO/Ag has the highest β factor, the tremendous metal damping loss arising from Ag film leads to much higher threshold. In the ZnO/MgO/Ag hybrid plasmonic structure, by the introduction of the MgO gap layer, the metal damping loss can be greatly reduced, resulting in lower threshold in comparison to the ZnO/Ag structure. Reducing the damping loss of the metallic cavities to an acceptable level is critical to realize electrically driven UV plasmonic lasers. Therefore, the thickness of the gap layer need be carefully designed, 7 nm in this work, to simultaneously reduce the metallic loss and preserve sufficiently strong confinement of electromagnetic field.

Metallic films supporting surface plasmon polaritons propagation can also be utilized as electrode for electrical injection of free carriers into the structure. When the p-GaN is biased positively, holes are injected into ZnO layer, and electrons are injected from Ag film through MgO gap layer. **Figure 4**a shows the current density–voltage characteristics of the plasmonic laser, exhibiting obvious rectifying behavior with a turn-on voltage of about 5.0 V. A typical emission image of the device is shown in the inset. Figure 4b presents the injection current density dependent emission spectra of the device detected from the lateral direction of the ZnO/MgO/Ag cavity (along x-axis in Figure 1a). At low injection current density (66.3 A cm^{-2}), only a relatively broad spontaneous emission peak centered at around 396 nm can be observed. When the injection current reaches 70.9 A cm^{-2}, a few sharp lasing peaks emerge at the shoulder of the spontaneous emission spectra, and the full width at half maximum (FWHM) of these sharp peaks is about 1.2 nm. The FWHM of the lasing peak in plasmonic laser is typically larger compared to conventional photonic ZnO laser[1c] due to its considerable metallic losses. The Q factor is estimated to 330 by $\lambda/\delta\lambda$, where λ and $\delta\lambda$ are the peak wavelength and the FWHM, respectively. On the other hand, Q factor also represents the ratio of the energy stored in the resonant cavity to the energy dissipated per cycle, which can be expressed by $Q = 2\pi/e^{-\alpha\lambda/n}$, where α is the total cavity loss and $L = 8$ μm is the FP cavity length. Using above parameters, α is estimated to be 3.9×10^5 cm^{-1}. New lasing peaks with orders-of-magnitude-higher than the underlying spontaneous emission appear at larger injection current, showing that the system have multi lasing mode behaviors. The lasing peaks show quasi-equidistant mode spacing of 2.74 nm, from which the effective index of the lasing modes is derived to be about 3.65. This value is in good agreement with the value of TM polarized modes in this structure obtained from numerical simulation (3.92), which further confirms that these lasing modes are TM polarized modes resulting from the strong light confinement of SPP. As the pumping power further increased to 79.4 A cm^{-2}, more modes appear together with the previous FP modes, as shown in Figure S5a in the Supporting Information. These new generated modes are very different from the FP modes as both their intensity and position are randomly change from one measurement to another, in contrast, the FP modes are reproducible in successive measurements, as shown in Figure S5b,c in the Supporting Information. This temporal chaotic behavior is the typical feature of random lasing modes, which have been extensively observed from ZnO materials. Since random lasing is relying on random scattering process, which leads to a high threshold, these random modes can only be observed at higher current injection density. Although a detailed study of this behavior is out of the scope of this concise report, our results show that these ZnO based plasmonic lasers are interesting devices to investigate dynamical effects and mode competition in plasmonic lasers. The line width variation of emission peaks and nonlinear response of the output power as function of the driving current confirm the realization of laser with a threshold of about 70.2 A cm^{-2} (Figure 4c). The output power of the device at 83.3 A cm^{-2} (40 mA) reaches 30 μW, which is amongst the best values ever reported for ZnO based lasers.[11a,14]

Figure 4d shows the far-field emission intensity as a function of angle with respect to the output facet of the ZnO/MgO/Ag cavity. The emission intensity reaches its maximum when θ is 0°, and decreases when the detector deviates from the normal of the cavity facet, as expected from a F–P lasing mode. The effective index of SPPs around the emission frequency (396 nm) is estimated to be 3.92 using FDTD. It is worth pointing out that the higher effective index of SPPs gives rise to high reflectivity ($R = 0.35$) of the two end-facets of the ZnO/MgO/Ag cavity, providing strong feedback for the plasmonic laser. In contrast, the reflectivity of the ZnO/air interfaces in conventional photonic cavities are roughly as low as $R \approx 0.18$. The total cavity loss inside this hybrid plasmonic structure, which is around 3.9×10^5 cm^{-1} as determined above, can also be expressed as: $\alpha = 1/L_m - 1/L\ln R$, where L_m^{-1} is the propagation loss of the plasmonic mode and $1/L\ln R$ represents

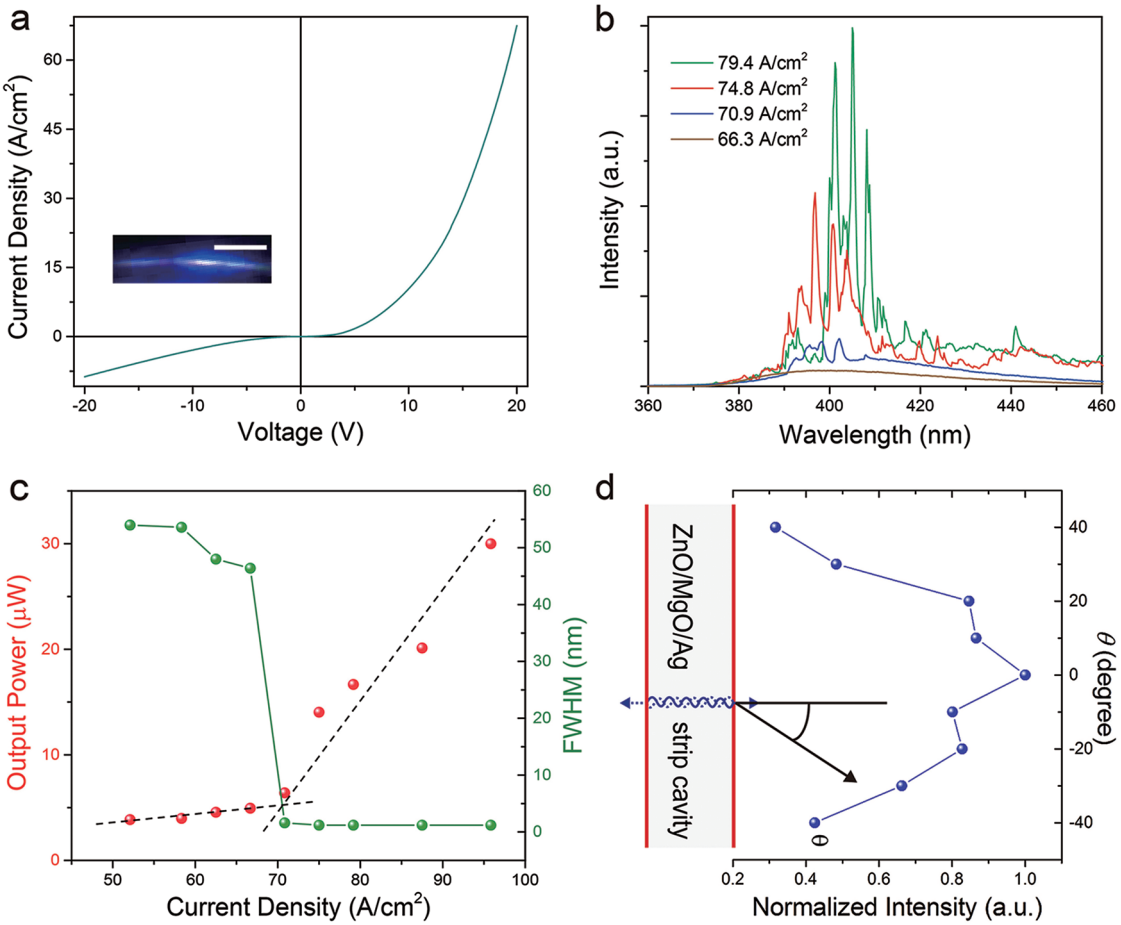

Figure 4. Lasing characteristics of the plasmonic laser. a) The current density–voltage characteristics of the plasmonic laser. The inset shows the emission image, and the scale bar is 100 μm. b) Injection current density dependent emission spectra of the plasmonic laser. c) The output power and line width of the emission peak versus injection current density. d) Angle distribution of the far-field emission intensity. The *y*-axis represents the emission angle θ with respect to the normal of the ZnO/MgO/Ag cavity and the *x*-axis represents the normalized emission intensity.

loss at the FP cavity facets.[1c] The cavity facets loss is calculated to be 1.31×10^3 cm^{-1}, which is two-orders-of-magnitude smaller than the total cavity loss. Therefore, one can see that the loss inside the plasmonic laser system mainly comes from the SPP propagation loss. Moreover, the thickness of both the MgO layer and the ZnO layer need to be designed carefully in such a way that the active region is close enough to the Ag layer surface, making sure that carriers in the ZnO layer can effectively couple with and transfer energy to SPPs, but also the MgO layer should be thick enough to effectively reduce the metallic losses. To illustrate this criterion, we have fabricated other devices according to the same structure but with a thicker MgO gap layer (15 nm). The latter exhibits a much larger threshold current of 301 A cm^{-2} (Figure S6a, Supporting Information). Increasing the MgO gap layer thickness greatly reduces the SPP- gain media energy transfer efficiency, leading to an increased threshold. Considering exciton-SPP transfer process, based on a dipole–dipole interaction model, the exciton-SPP energy transition rate can be expressed by the following formula[7a]

$$R_{\text{ex-SPPs}} \approx A/d^6 \quad (1)$$

where A is a constant for a given system, and d is the distance between excitons and surface plasmons decreasing rapidly as function of the thickness, in agreement with the obtained experimental results. Meanwhile, we also observed that due to the large metallic losses, no lasing can be achieved when the MgO gap layer thickness is reduced below 5 nm. Varying the thickness of ZnO layer also modifies the exciton-SPP energy transfer efficiency due to the change of the distance between active region and Ag surface plasmon. Another design with 120 nm ZnO layer and 7 nm MgO gap layer have been investigated under the same experimental conditions. These devices exhibit thresholds of 185 A cm^{-2} (Figure S6b, Supporting Information), relatively larger than that of the device with 85 nm ZnO layer (70.2 A cm^{-2}). Although increasing the ZnO thickness increases the "photonic" portion of the structure, we confirm from mode spacing and threshold behaviors the role of SPPs modes in the lasing action.

In this configuration, SPPs are highly polarized. We have also examined the polarization behaviors of lasing emission using an optical analyzer plate to filter out the perpendicular electric field component. **Figure 5**a shows TM and TE mode spectra of the plasmonic laser above threshold (70.9 A cm^{-2}).

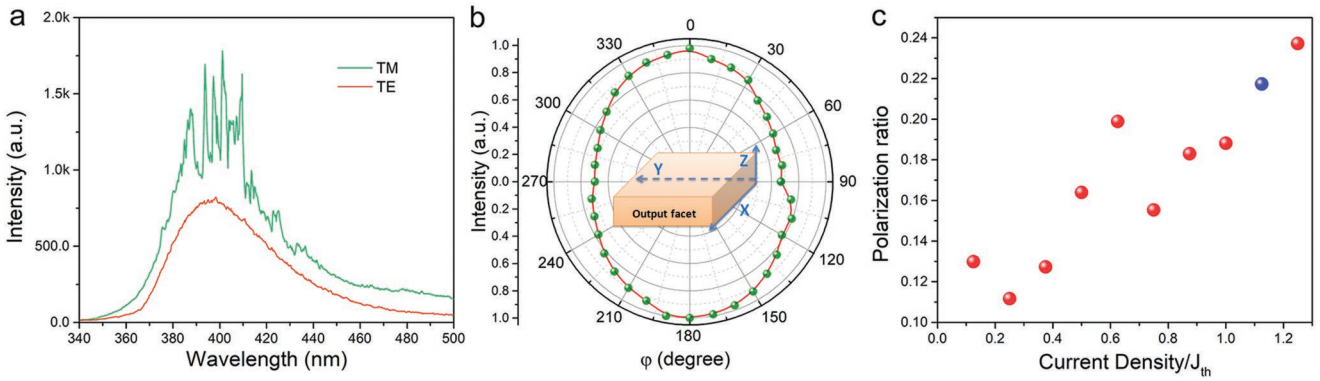

Figure 5. Laser emission polarization. a) Emission spectra of the TE and TM modes. b) The corresponding polar plot of the emission intensity. The polarization direction is perpendicular to the Ag film with a polarization ratio of 0.22. c) Polarization ratio variation versus injection normalized to the threshold current density (J_{th}). The blue point indicates injection current at which the spectra in (a) and polar plot in (b) were recorded.

The emission intensity of the TM component (red curve) is obviously stronger than the TE component (blue curve), and clear lasing modes can only be detected from the TM component. The polarization anisotropy can be described by the polarization ratio $\rho = (I_{\perp} - I_{\parallel})/(I_{\parallel} + I_{\perp})$,[15] leading to a polarization ratio of ≈0.22. Figure 5b shows the corresponding polar plot of the emission intensity. Considering that other factors such as interface reflection may also lead to polarized light emission, the dependence of polarization ratio on injection current has been investigated in order to identify the origin of the polarized emissions from this structure, as shown in Figure 5c. It can be seen that the polarization ratio of this structure increases as increasing the driving current. This behavior is very different from the polarized emissions caused by interface reflection which is independent on emission intensity or driving current, and therefore confirms that the polarized lasing mode belongs to the fundamental surface plasmon mode.

3. Conclusions

In conclusion, we have demonstrated electrically driven UV plasmonic lasers operating at room temperature for the first time. The realization of the UV plasmonic lasers is attributed to the strong confinement of light into surface plasmon polaritons at the interface between a semiconductor and Ag film. We experimentally prove that electrically driven UV plasmonic lasing at room temperature is achievable after carefully addressing the metallic loss by incorporating a MgO gap layer. Comparing electrically versus optically pumped plasmonic lasing, we observed that the emission wavelengths redshift as a function of the injected carrier density, while it blueshifts for optical pumping, as evidenced from Figure 4b and Figure S4c in the Supporting Information. Although the change in the emission behavior might be related to different operation regime, it is difficult to dissociate the effect of bandgap renormalization due to EHP inducing redshifted emission versus the temperature dependent laser emission properties imposed by the large ohmic losses resulting from the injection of electrical current. Localizing light in subwavelength dimension, these new types of UV plasmonic nanolasers may find interesting applications in photolithography, sensing, and integrated microfluidic systems for surface sterilizations and various nanoscale treatment processes.

4. Experimental Section

Electrical injection in p-GaN/MgO/ZnO/MgO/Ag plasmonic lasers imposes stringent structural properties on the different layers. A 5 nm MgO layer was first deposited onto the p-GaN substrate at low substrate temperature (400 °C) in molecular beam epitaxy (MBE) system. Then the substrate temperature was raised to 650 °C for the following growth of 85 nm ZnO layer and 7 nm MgO gap layer. To compare the performances of devices, ZnO layer and MgO gap layer of different thickness were deposited by varying the growth time. The thickness, hole concentration, and Hall mobility of the p-GaN were 2 µm, 3.6×10^{17} cm^{-3}, and 8.4 cm^2 V^{-1} s^{-1}, respectively. The unintentionally doped ZnO layer showed n type conduction, with electron concentration and Hall mobility of about 1.5×10^{16} cm^{-3}, and 70.6 cm^2 V^{-1} s^{-1}, respectively. After that, an Ag planar waveguides with 8 µm in width, 300 µm in length connected to a 300 µm × 300 µm Ag electrode, was thereafter fabricated by photolithography technique, and the Ag film with a thickness of 100 nm was deposited using magnetron sputtering. At last, the p-GaN/MgO/ZnO/MgO/Ag waveguide cavity was defined by chemical etching in dilute hydrochloric acid (1%) for 10 s. Chemical etching also helped reducing the interface roughness, increasing the *Q*-factor of the plasmonic cavity. Ni/Au electrode was evaporated onto the p-GaN as p contact.

All the measurements were carried out at room temperature. The device was forward biased with a d.c. current source, placed on a copper plate for cooling during electroluminescence measurements. To carry out PL spectra and ultrafast transient absorption measurements, ZnO, ZnO/Ag, and ZnO/MgO/Ag structures were prepared onto sapphire substrate at the same growth conditions. The samples were pumped using monochromatic laser pulses (λ = 340 nm, FWHM 100 fs, 1 kHz repetition rate) and the probe white light is generated by exciting a CaF_2 window with 5 mm thickness. Pump and probe beams have diameters of 500 and 300 µm at the sample. The same laser pulses were utilized in photoluminescence measurements. The Ag layer in the ZnO/MgO/Ag structure used to characterize the transient absorption was 30 nm in thickness, thus sufficiently thin compared to the skin depth to transmit the probe beam through the sample. The energy of the pump pulses was tuned by a variable neutral density filter. The pump pulses were chopped by a synchronized chopper to 500 Hz. The schematic of the experiment is shown in Figure S1 in the Supporting Information.

Supporting Information

Supporting Information is available from the Wiley Online Library or from the author.

Acknowledgements

X.Y. and P.-N.N. contributed equally to this work. The authors acknowledge useful discussions with J. M. Chauveau and F. Semond. This research has been partially supported by European Research Council (ERC) under the European Union's Horizon 2020 research and innovation program (grant agreement FLATLIGHT No 639109), and the Natural Science Foundation of China (61804136, 61604132, and U1604263), and the National Science Foundation for Distinguished Young Scholars of China (61425021).

Conflict of Interest

The authors declare no conflict of interest.

Keywords

plasmonic lasers, surface plasmon polaritons, zinc oxide

Received: December 3, 2018
Revised: February 1, 2019
Published online: March 15, 2019

[1] a) Y. H. Chou, B. T. Chou, C. K. Chiang, Y. Y. Lai, C. T. Yang, H. Li, T. R. Lin, C. C. Lin, H. C. Kuo, S. C. Wang, *ACS Nano* **2015**, *9*, 3978; b) R. F. Oulton, *Mater. Today* **2012**, *15*, 26; c) R. M. Ma, R. F. Oulton, V. J. Sorger, X. Zhang, *Laser Photonics Rev.* **2013**, *7*, 1; d) C. Y. Wu, C. T. Kuo, C. Y. Wang, C. L. He, M. H. Lin, H. Ahn, S. Gwo, *Nano Lett.* **2011**, *11*, 4256.

[2] a) M. T. Hill, Y. S. Oei, B. Smalbrugge, Y. Zhu, T. De Vries, P. J. Van Veldhoven, F. W. M. Van Otten, T. J. Eijkemans, J. P. Turkiewicz, H. De Waardt, *Nat. Photonics* **2007**, *1*, 589; b) H. G. Park, Y. H. Lee, *Science* **2004**, *305*, 1444; c) S. L. Mccall, A. F. J. Levi, R. E. Slusher, S. J. Pearton, *Appl. Phys. Lett.* **1992**, *60*, 289; d) K. Nozaki, T. Baba, *Appl. Phys. Lett.* **2006**, *88*, 211101; e) T. Tao, T. Zhi, B. Liu, J. Dai, Z. Zhuang, Z. Xie, P. Chen, F. Ren, D. Chen, Y. Zheng, R. Zhang, *Adv. Funct. Mater.* **2017**, *27*, 1703198.

[3] a) B. Smalbrugge, C. Z. Ning, E. J. Geluk, E. S. P. Leong, F. Karouta, M. T. Hill, M. K. Smit, M. Marell, M. Sun, P. J. V. Veldhoven, *Opt. Express* **2009**, *17*, 11107; b) M. A. Noginov, G. Zhu, A. M. Belgrave, R. Bakker, V. M. Shalaev, E. E. Narimanov, S. Stout, E. Herz, T. Suteewong, U. Wiesner, *Nature* **2009**, *460*, 1110; c) R. F. Oulton, V. J. Sorger, T. Zentgraf, R. M. Ma, C. Gladden, L. Dai, G. Bartal, X. Zhang, *Nature* **2009**, *461*, 629; d) S. H. Kwon, J. H. Kang, C. Seassal, S. K. Kim, P. Regreny, Y. H. Lee, C. M. Lieber, H. G. Park, *Nano Lett.* **2010**, *10*, 3679; e) M. I. Stockman, *J. Opt.* **2010**, *12*, 024004.

[4] P. Berini, I. D. Leon, *Nat. Photonics* **2012**, *6*, 16.

[5] a) J. N. Anker, W. P. Hall, O. Lyandres, N. C. Shah, J. Zhao, R. P. Van Duyne, *Nat. Mater.* **2008**, *7*, 442; b) J. Homola, *Chem-Inform* **2008**, *39*, 462; c) S. Kawata, Y. Inouye, P. Verma, *Nat. Photonics* **2009**, *3*, 388; d) W. L. Barnes, A. Dereux, T. W. Ebbesen, *Nature* **2003**, *424*, 824; e) D. K. Gramotnev, S. I. Bozhevolnyi, *Nat. Photonics* **2010**, *4*, 83.

[6] R. F. Oulton, V. J. Sorger, D. A. Genov, D. F. P. Pile, X. Zhang, *Nat. Photonics* **2008**, *2*, 496.

[7] a) Q. Zhang, G. Li, X. Liu, F. Qian, Y. Li, T. C. Sum, C. M. Lieber, Q. Xiong, *Nat. Commun.* **2014**, *5*, 4953; b) M. P. Nezhad, A. Simic, O. Bondarenko, B. Slutsky, A. Mizrahi, L. Feng, V. Lomakin, Y. Fainman, *Nat. Photonics* **2010**, *4*, 395; c) R. M. Ma, R. F. Oulton, V. J. Sorger, G. Bartal, X. Zhang, *Nat. Mater.* **2011**, *10*, 110.

[8] T. P. H. Sidiropoulos, R. Röder, S. Geburt, O. Hess, S. A. Maier, C. Ronning, R. F. Oulton, *Nat. Phys.* **2014**, *10*, 870.

[9] A. B. Djurišić, A. M. C. Ng, X. Y. Chen, *Prog. Quantum Electron.* **2010**, *34*, 191.

[10] A. O. Govorov, J. Lee, N. A. Kotov, *Phys. Rev. B* **2009**, *76*, 125308.

[11] a) X. Yang, L. Dong, C. Shan, J. Sun, N. Zhang, S. Wang, M. Jiang, B. Li, X. Xie, D. Shen, *Adv. Mater.* **2017**, *29*, 1602832; b) H. Zhu, C. X. Shan, B. Yao, B. H. Li, J. Y. Zhang, Z. Z. Zhang, D. X. Zhao, D. Z. Shen, X. W. Fan, Y. M. Lu, *Adv. Mater.* **2009**, *21*, 1613.

[12] a) Y. H. Chou, Y. M. Wu, K. B. Hong, B. T. Chou, J. H. Shih, Y. C. Chung, P. Y. Chen, T. R. Lin, C. C. Lin, S. D. Lin, *Nano Lett.* **2016**, *16*, 3179; b) Y. J. Lu, J. Kim, H. Y. Chen, C. Wu, N. Dabidian, C. E. Sanders, C. Y. Wang, M. Y. Lu, B. H. Li, X. Qiu, W. H. Chang, L. J. Chen, G. Shvets, C. K. Shih, S. Gwo, *Science* **2012**, *337*, 450.

[13] a) R. Röder, M. Wille, S. Geburt, J. Rensberg, M. Zhang, J. G. Lu, F. Capasso, R. Buschlinger, U. Peschel, C. Ronning, *Nano Lett.* **2013**, *13*, 3602; b) U. Ozgur, Y. I. Alivov, C. Liu, A. Teke, M. A. Reshchikov, S. Dogan, V. Avrutin, S. J. Cho, H. Morkoc, *J. Appl. Phys.* **2005**, *98*, 041301.

[14] a) X. Y. Liu, C. X. Shan, S. P. Wang, Z. Z. Zhang, D. Z. Shen, *Nanoscale* **2012**, *4*, 2843; b) J. Huang, S. Chu, J. Y. Kong, L. Zhang, C. M. Schwarz, G. P. Wang, L. Chernyak, Z. H. Chen, J. L. Liu, *Adv. Opt. Mater.* **2013**, *1*, 179; c) S. Chu, G. Wang, W. Zhou, Y. Lin, L. Chernyak, J. Zhao, J. Kong, L. Li, J. Ren, J. Liu, *Nat. Nanotechnol.* **2011**, *6*, 506; d) A. O. Govorov, J. Lee, N. A. Kotov, *Phys. Rev. B* **2007**, *76*, 125308.

[15] W. Jianfang, M. S. Gudiksen, D. Xiangfeng, C. Yi, C. M. Lieber, *Science* **2001**, *293*, 1455.